


Article

An Improved Droop Control Scheme of a Doubly-Fed Induction Generator for Various Disturbances

Yien Xu ¹, Pei Chen ¹, Xinsong Zhang ^{1,*} and Dejian Yang ^{2,*} 

¹ School of Electrical Engineering, Nantong University, Nantong 226019, China; 2011310014@stmail.ntu.edu.cn (Y.X.); 2011310026@stmail.ntu.edu.cn (P.C.)

² Key Laboratory of Modern Power System Simulation and Control & Renewable Energy Technology, Ministry of Education, Northeast Electric Power University, Jilin 132012, China

* Correspondence: zhang.xs@ntu.edu.cn (X.Z.); dejian@ntu.edu.cn (D.Y.); Tel.: +86-1585-125-4360 (X.Z.)

Abstract: Doubly-fed induction generators (DFIGs) participate in the system frequency regulation using a fixed-coefficient droop control scheme. Nevertheless, the frequency-supporting capability of this control scheme with fixed gain is limited for different disturbances. This paper suggests an improved droop control scheme for a DFIG that can both alleviate the frequency nadir and maximum rate of change of frequency (ROCOF) during the frequency regulation. To achieve this, an adaptive droop control coefficient based on the ROCOF is suggested. The proposed droop control coefficient is a linear function of the ROCOF. Therefore, the proposed scheme can adjust the control coefficient according to the varying ROCOF. Simulation results clearly demonstrate that the proposed droop control scheme shows better effectiveness in improving the maximum ROCOF and frequency nadir under various sizes of disturbance, even in a varying wind speed.

Keywords: doubly-fed induction generator; adaptive droop coefficient; wind power; frequency nadir; ROCOF



Citation: Xu, Y.; Chen, P.; Zhang, X.; Yang, D. An Improved Droop Control Scheme of a Doubly-Fed Induction Generator for Various Disturbances. *Energies* **2021**, *14*, 7980. <https://doi.org/10.3390/en14237980>

Academic Editors: Ioana Pisica, Sumit Paudyal and Oguzhan Ceylan

Received: 25 October 2021

Accepted: 25 November 2021

Published: 29 November 2021

Publisher's Note: MDPI stays neutral with regard to jurisdictional claims in published maps and institutional affiliations.



Copyright: © 2021 by the authors. Licensee MDPI, Basel, Switzerland. This article is an open access article distributed under the terms and conditions of the Creative Commons Attribution (CC BY) license (<https://creativecommons.org/licenses/by/4.0/>).

1. Introduction

With the increasingly serious problems of energy shortage and environmental pollution, renewable energy power generation represented by wind power has developed rapidly [1]. However, due to the randomness and fluctuation characteristics of wind power generation, the stability of the system frequency is significantly threatened [2,3]. Further, the reduction in inertia level and frequency regulation capability of the electric power system becomes severe since a large amount of traditional synchronous generators (TSGs) are replaced by wind turbine generators (WTGs) [4–6]. As a result, the frequency quality indexes including the maximum rate of change of frequency (ROCOF, df/dt) and frequency nadir (FN) would be worse, and severe disturbance will lead to large-scale wind power off grid and lead to more serious chain problems [7,8]. As studied in [9,10], the frequency support capability from a WTG can be several times higher than that of a TSG. In addition, WTGs are able to improve the FN and the maximum ROCOF with frequency regulation schemes [11–14]. Therefore, some countries have released the specific requirements of the participation in frequency regulation for WTGs [15,16].

To meet the system frequency response requirements, when detecting a frequency event, additional control loops (df/dt -based inertia control, Δf -based inertia control) are added to the WTGs [17–22]. The decoupling control scheme was suggested in [20]; it can successfully improve the frequency nadir, but the incremental power is less during the initial stage of the disturbance so that the benefit of improving the maximum df/dt is limited. The authors in [21] suggested an optimal frequency control scheme of the wind turbine generator and coordinated with synchronous generators. However, for various conditions, the control coefficients should be tuned. The capability of providing inertia and primary frequency support scheme was evaluated in [22]. Nowadays, these existing

frequency-regulating strategies are roughly divided into two types: ROCOF-based inertia control [23] and frequency deviation-based inertia control [24]. The study in [25] indicated that WTGs can emulate inertia response of TSGs with the ROCOF-based frequency control loop. The authors of [26] addressed employing the maximum df/dt for achieving the inertial response emulated control of the DFIG. In [27], the benefits of ROCOF-based inertia control scheme from the DFIG are investigated with different control gains.

Droop control, which simulates the active power frequency droop characteristics of TSGs, has been widely studied and applied [28]. The authors of [29] suggested that the output of WTGs to support the system frequency could be controlled according to the droop curve between generator electromagnetic torque and system frequency. In [30], the performances of droop control scheme with different fixed-coefficients were investigated. It clearly illustrated that WTGs with a large coefficient show better performance in frequency support capability, while the stalling of the rotor speed is inevitable since too much kinetic energy is released; a small coefficient can avoid the stall of the rotor speed, but less contribution of the kinetic energy is devoted to improving the FN. The authors of [31] suggested a time-varying parameter droop control strategy considering the effective rotational kinetic energy of DFIG, which can effectively enhance the system frequency stability and prevent the stalling of wind turbines under different wind speeds. However, the conventional droop control strategy of the wind turbine mainly affects the frequency nadir of system frequency response, and has little effect on the ROCOF. In the above strategies, the setting of droop control coefficient is determined with the operation state of WTGs, and the research on parameter setting methods under various disturbances is inadequate.

Based on the droop control scheme with fixed coefficient, this study advances an adaptive droop control strategy for a DFIG that improves the maximum ROCOF and frequency nadir under various disturbances. In this strategy, a novel droop control coefficient based on the ROCOF is suggested. Due to the positive relationship between the ROCOF and disturbance, the proposed droop control strategy can adjust the value of the control coefficient flexibly for various disturbances. Furthermore, DFIGs are assumed to operate at MPPT mode prior to a frequency event. The performances of the enhanced droop control strategy are investigated with various disturbances and wind conditions by EMT-PV simulator.

2. Modeling of a Doubly-Fed Induction Generator

The DFIG control system used in this study comprises a pitch controller, rotor-side converter (RSC) controller, and grid-side converter (GSC) controller (see Figure 1). The pitch controller focuses on preventing the excessive rotor speed. RSC controller keeps the stator voltage at a desirable reference, adjusts the active power injected into the power grid, and realizes the maximum power point tracking (MPPT) operation for DFIG. The DC-link voltage is maintained at a stable value by the GSC controller.

The mechanical power captured by a DFIG from the flowing air (P_m) can be expressed as:

$$P_m = 0.5\rho S v_w^3 c_p \quad (1)$$

where ρ and S means the air density and swept area, respectively. v_w indicates the speed of the flowing air. c_p represents the power coefficient [2].

As in [2], c_p is a nonlinear function of the pitch angle (β) and tip-speed ratio (λ), and its expression is given by:

$$c_p(\lambda, \beta) = 0.645 \left\{ 0.00912\lambda + \frac{-5 - 0.4(2.5 + \beta) + 116\lambda_i}{e^{21\lambda_i}} \right\} \quad (2)$$

where:

$$\lambda_i = \frac{1}{\lambda + 0.08(2.5 + \beta)} - \frac{0.035}{1 + (2.5 + \beta)^3} \quad (3)$$

$$\lambda = \frac{\omega_r R}{v_w} \quad (4)$$

where ω_r and R are the rotor angular velocity and blade length, respectively.

As in [32], c_p exists a maximum value ($c_{p, \max}$) when λ is at the optimal tip-speed ratio (λ_{opt}), where the pitch angle (β) is zero, the power reference for the MPPT operation, P_{MPPT} , is expressed as:

$$P_{MPPT} = \frac{1}{2} C_{p, \max} \rho \pi R^2 \left(\frac{\omega_r R}{\lambda_{opt}} \right)^3 = k_g \omega_r^3 = 0.512 \omega_r^3 \quad (5)$$

$$k_g = \frac{1}{2 \lambda_{opt}^3} C_{p, \max} (\lambda_{opt}, 0) \rho \pi R^5 \quad (6)$$

where k_g is a constant calculating by (6) and is 0.512.

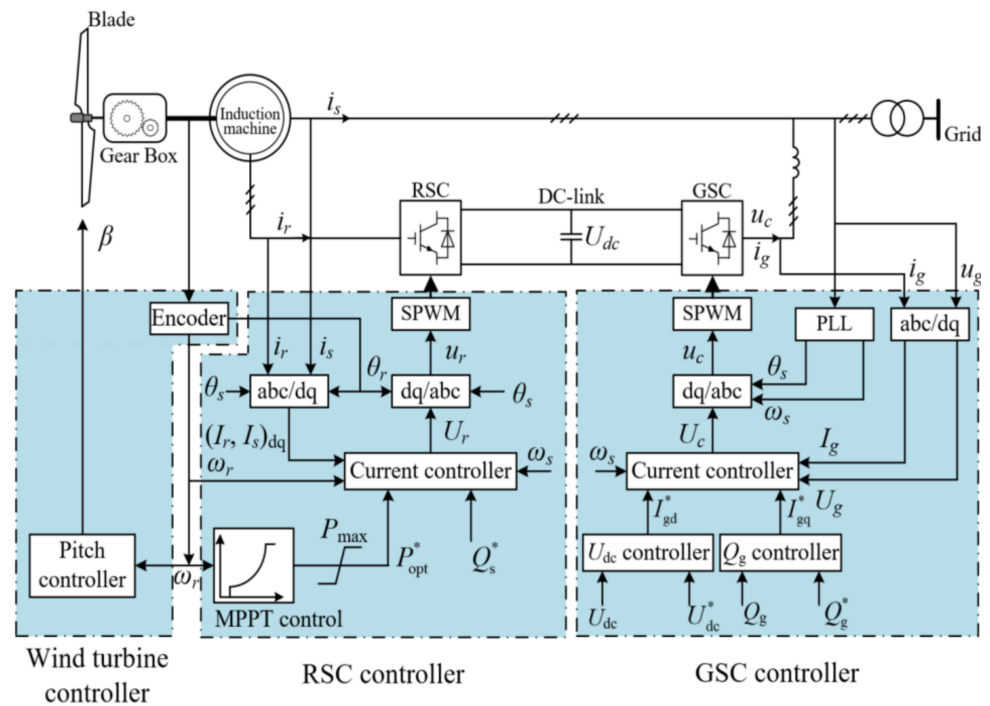


Figure 1. Typical structure of a DFIG and its controllers.

A two-mass shaft model is employed to display the mechanical dynamics between the wind turbine and generator in this paper, as given by:

$$2H_t \frac{d\omega_t}{dt} = T_m - T_{ls} \quad (7)$$

$$2H_g \frac{d\omega_r}{dt} = T_{hs} - T_{em} \quad (8)$$

$$T_{ls} = K\theta_s + D(\omega_t - \omega_{ls}) \quad (9)$$

where T_m means the mechanical torque from the turbine. T_{em} is the generator electrical torque. H_t and H_g are the turbine inertia constant and generator inertia constant, respectively. T_{ls} and T_{hs} are the torques of the low-speed and high-speed shafts, respectively. ω_t is the turbine rotor speed. ω_r is the generator rotor speed. K is the spring constant. θ_s is the torsional twist. D is the damping constant. ω_{ls} is the rotor angular velocity of the low-speed shaft [33].

3. Proposed Adaptive Droop Control Scheme of a DFIG

Figure 2 illustrates the control concept of the droop control. Upon detecting a frequency event, the output of the DFIG switches to droop control mode using an additional control loop. The power reference for the droop control (P_{ref}) is represented by (10), which comprises MPPT operation and the output of droop control. Thus, the frequency response capability of the DFIG for droop control is critically dependent on the droop coefficient:

$$P_{ref} = P_{MPPT} + \Delta P_{droop} = P_{MPPT} + K_{AG} \times \Delta f \quad (10)$$

where P_{MPPT} is the output of MPPT operation. ΔP_{droop} indicates the incremental power for the droop control loop. K_{AG} means the adaptive gain. Δf is the frequency deviation.

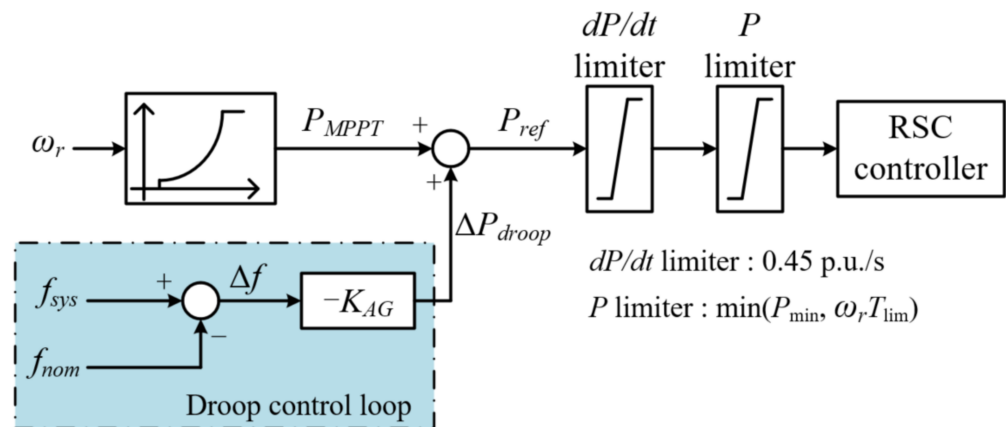


Figure 2. Control concept of the droop control.

As mentioned in [19], the conventional droop control with fixed control coefficient is unable to provide enough frequency response service under various disturbances (see Figure 3). Moreover, the conventional droop control coefficient of the wind turbine mainly affects the frequency nadir of system frequency response, and has little effect on the ROCOF. This paper aims to design an adaptive droop control coefficient to reduce both the maximum frequency deviation and ROCOF effectively. To achieve this, the droop control coefficient is coupled with the ROCOF so as to regulate the control coefficient according to the ROCOF and further improves the frequency-regulating capability of the DFIG under various disturbances, the proposed adaptive droop control coefficient can be represented by:

$$K_{AG}(df/dt) = K_0 + k_1 \times \left(\left| \frac{df}{dt} \right|^n \right) \quad (11)$$

where K_0 is the basic control coefficient for the droop control; k_1 is the droop control factor, which can regulate the performance of improving the frequency supporting capability for the DFIG. n is a quotient to achieve first-order, second-order or other order functions.

In the conventional scheme, the control coefficient is set to 20, which is the same as the basic control coefficient of the proposed scheme (K_0) in (11). In addition, k_1 in (11) is the control factor and is used to regulate the performance of improving the frequency supporting capability for the DFIG. Thus, when the df/dt is equal to zero, the proposed adaptive control coefficient is the same as the control coefficient in the conventional scheme. As the absolute value of df/dt increases, the proposed control coefficient is more than it in the conventional scheme, as a result, the calculated incremental power and power reference for the DFIG is more than in the conventional scheme. Thus, the proposed control scheme can improve the frequency support capability. The control coefficient of the conventional scheme, K_0 and k_1 can be set to different values according to the design objectives.

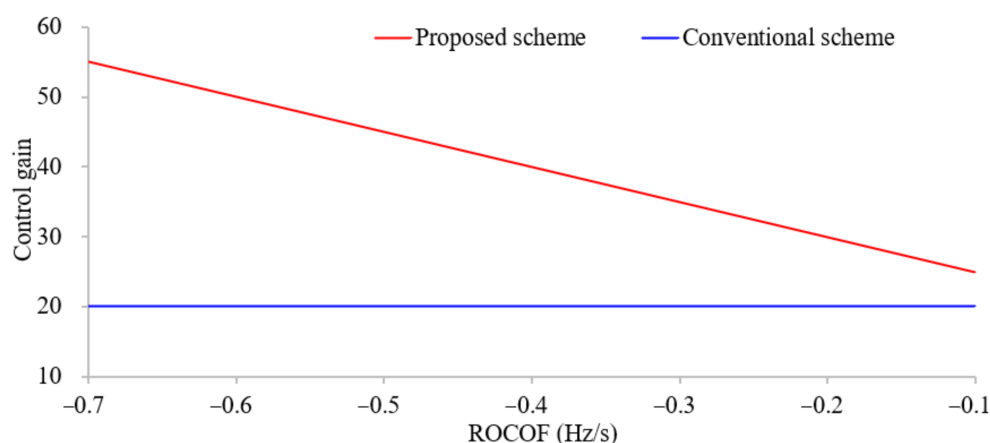


Figure 3. Comparison of proposed and conventional droop coefficients.

Figure 3 shows the droop coefficients of the proposed and conventional strategies; the control coefficient for the conventional scheme is a constant value for the various ROCOFs. On the contrary, the control coefficient for the proposed droop control strategy could regulate with different ROCOFs (see Equation (10)). In addition, the maximum ROCOF is positively correlated with the disturbance occurs at the beginning of a frequency disturbance [34,35]. Therefore, the DFIG implemented with the proposed scheme generates more power compared with the conventional scheme. Hence, the proposed droop control strategy can further heighten the FN and alleviate the maximum ROCOF under various disturbances.

4. Model System

To verify the efficacy of the droop control scheme, three cases with various sizes of disturbance and wind conditions are carried out using the model system shown in Figure 4. As a disturbance, SG₄ is tripped out at 40 s.

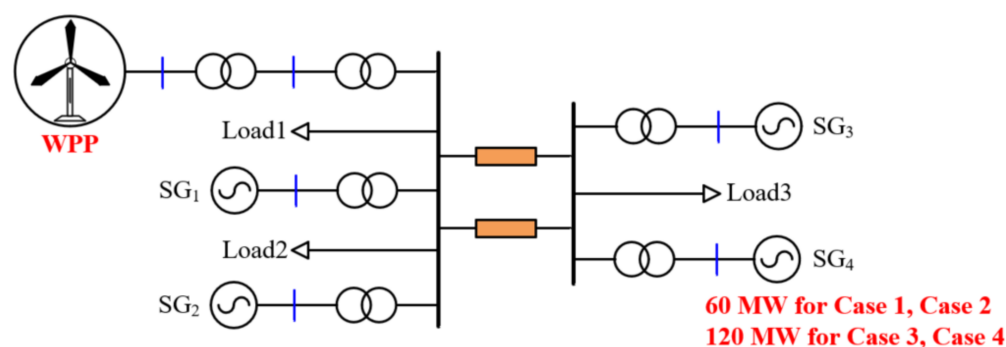


Figure 4. Model system embedded with a DFIG-based WPP.

4.1. Conventional Synchronous Generators

As displayed in Figure 4, four conventional SGs with the IEEE G1 steam governor model are used in the model system, which are two 100-MVA SGs and two 200-MVA SGs, respectively. In addition, as in [36], the droop coefficient of TSG is usually varying from 3–5%. In order to model a power system with a low ramping capability, the droop coefficients of all SGs are set to 5% in this study. Figure 5 shows the typical structure of the IEEE G1 steam governor model. Furthermore, the inertia time constant is basically proportional to the capacity of the SG and the inertia time constants of the SGs are set to 4 s for 100 MVA and 5 s for 200 MVA, respectively [8,37].

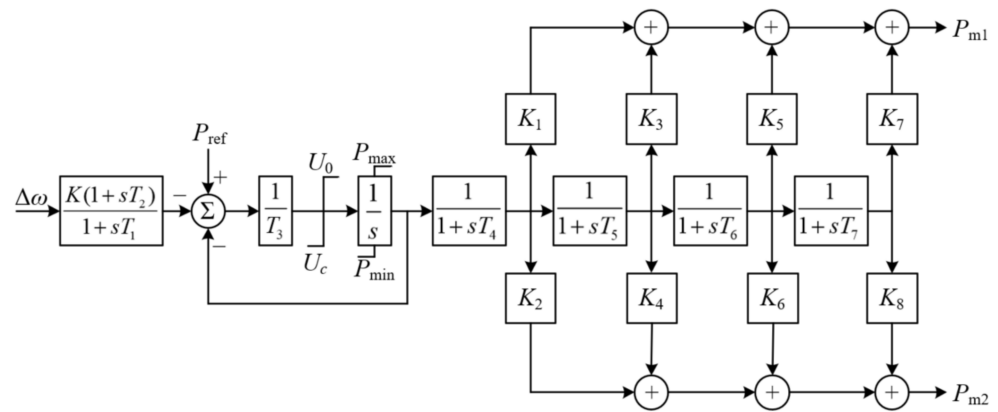


Figure 5. IEEE1 steam governor model.

4.2. DFIG-Based Wind Power Plant

The detailed description of the model for DFIG can be achieved in Section 3. In addition, to avoid the excessive active power and prevent the DFIG from mechanical fatigue, the maximum power and rate limiters are employed in this study, as in [8].

5. Case Studies

In this section, Case 1 is carried out to investigate the relationship between different coefficient expressions and their control performance. Since the system frequency indexes (frequency nadir and maximum ROCOF) are different under various sizes of frequency disturbances, the performances of the proposed droop control scheme by various disturbances are investigated in Case 2 (wind speed of 8.5 m/s, disturbance of 60 MW) and Case 3 (wind speed of 8.5 m/s, disturbance of 120 MW), respectively. Considering the wind speeds are varying in a realistic scenario, the performance of the proposed droop control strategy is investigated under a random wind speed (Case 4: random wind conditions, disturbance of 120 MW). The performance of the proposed scheme is compared with that of MPPT operation and the droop control scheme with fixed control coefficient (conventional scheme), as in [19]. In addition, the values of K_0 and k_1 in (11) are set to 20 and 50, respectively. The control coefficient of the conventional scheme is set to 20, which is same as K_0 .

5.1. Case 1: Wind Speed of 8.5 m/s, Disturbance of 60 MW with Various Settings of Quotient

Figure 6 displays the simulation results (to show the relationship between different coefficient expressions and their control performance), where K_{AG} is a first-order, second-order, and third-order function of df/dt , respectively. The frequency nadirs for a third-order and second-order function of df/dt are 59.508 Hz and 59.507 Hz, respectively (see Figure 6a). The frequency nadir in the proposed strategy where K_{AG} is a first-order function of df/dt is 59.519 Hz, which is greater than that of other order functions by 0.011 Hz and 0.012 Hz, respectively. This is mainly because the second polynomial in (10) is inverse-proportional to the setting of n so that a larger amount of active power of the wind turbine is injected to the power grid under a first-order function (see Figure 6b); as a result, the reduction in the rotor speed is large (see Figure 6c). In addition, the maximum ROCOFs for the first-order, second-order, and third-order functions of df/dt are -0.430 Hz/s, -0.437 Hz/s, and -0.439 Hz/s, respectively. Consequently, the performances of alleviating the frequency nadir and maximum ROCOF with a first-order function of df/dt are better compared to others functions of df/dt , the setting of n has nonlinear relationship with the control performance. Thus, in the following cases, n in (10) is set to 1 to obtain the better performance.

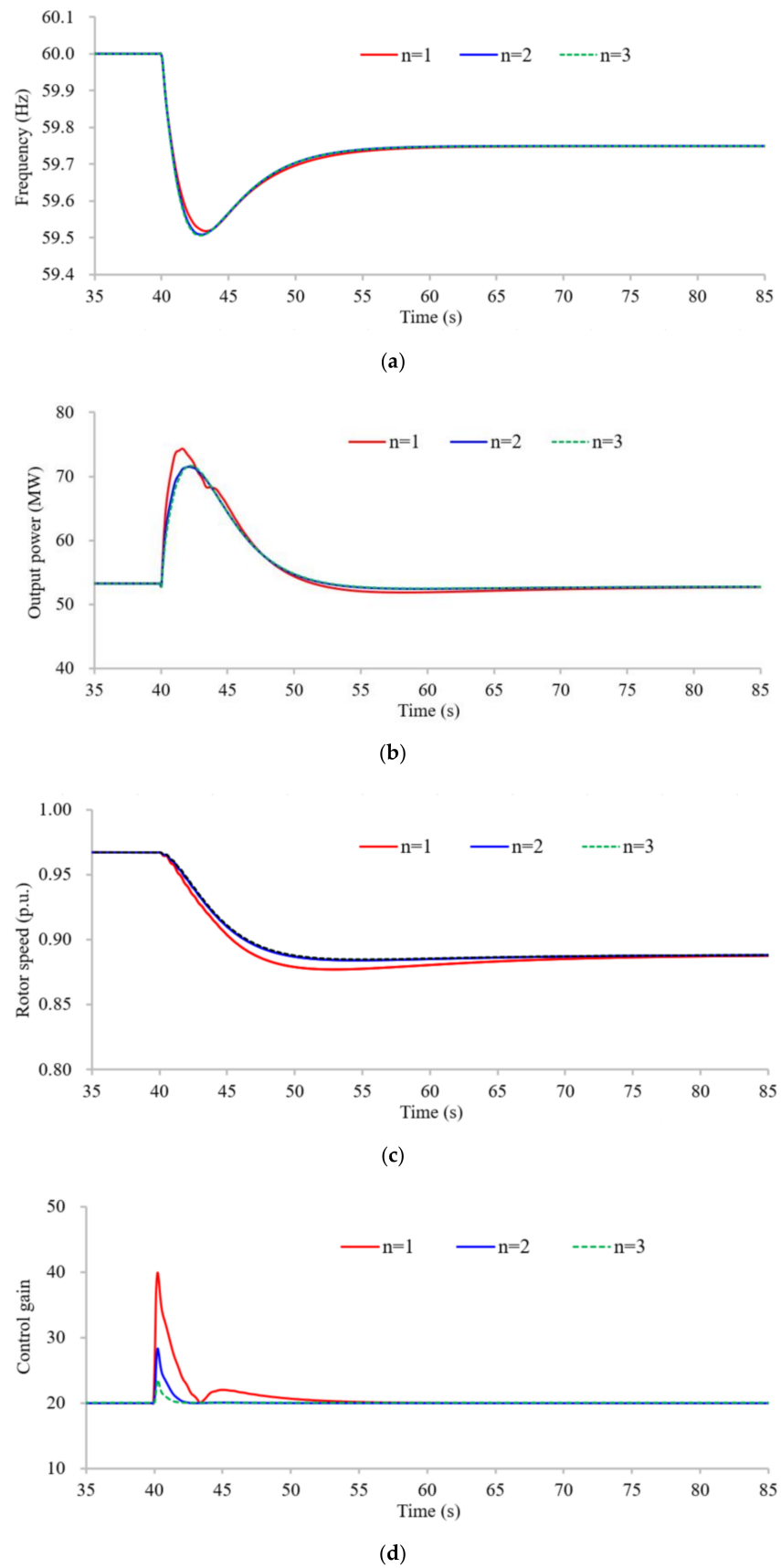


Figure 6. Simulation results for Case 1: (a) System frequencies; (b) Active power of the DFIG; (c) Rotor speeds; (d) Control coefficients.

5.2. Case 2: Wind Speed of 8.5 m/s and Disturbance of 60 MW

Figure 7 shows the system frequencies, active power, rotor speeds, and control coefficients of DFIG for Case 2.

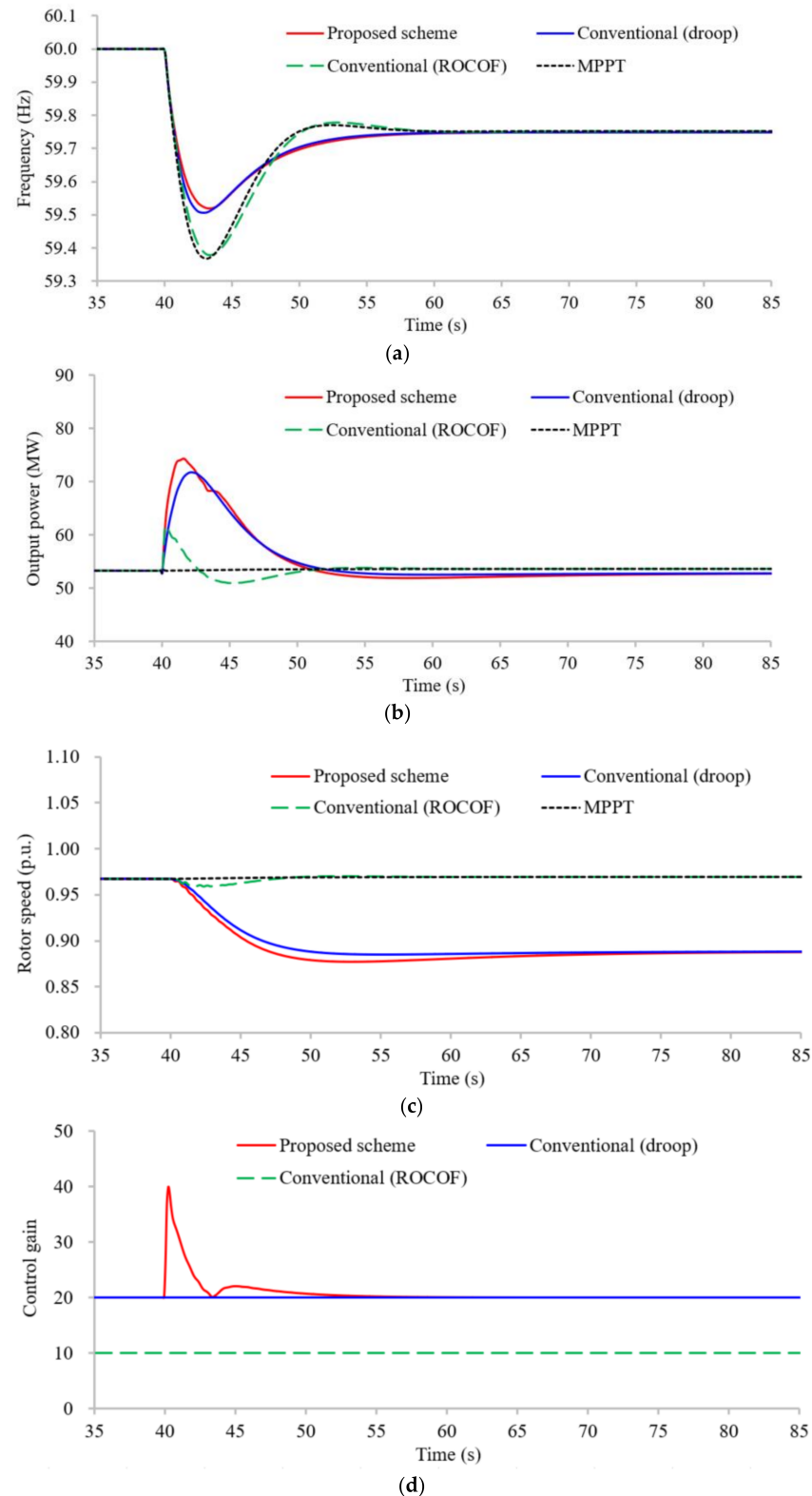


Figure 7. Simulation results for Case 2: (a) System frequencies; (b) Active power of the DFIG; (c) Rotor speeds; (d) Control coefficients.

In MPPT operation, the frequency nadir is 59.367 Hz. Compared with MPPT operation, the maximum ROCOF and FN for the conventional (droop) scheme and conventional (ROCOF) scheme are increased to 59.507 Hz and 59.379 Hz, respectively, because an amount of kinetic energy is injected into the power grid using the fixed control coefficient (see Figure 7a,b). Since a larger amount of active power is injected to the power grid (see Figure 7a), the frequency nadir of the proposed scheme is 59.519 Hz, which is greater than that of the conventional (droop) scheme and conventional (ROCOF) scheme by 0.012 Hz and 0.140 Hz, respectively.

The maximum ROCOFs for the conventional (droop) and cs are -0.441 Hz/s and -0.428 Hz/s, respectively. Compared with conventional (droop) scheme, the maximum ROCOF in the proposed scheme is -0.431 Hz/s, improved by which is greater than that of the conventional (droop) scheme by -0.010 Hz/s, but it is slightly lower than conventional (ROCOF) scheme. This is mainly because a greater active power is obtained at the beginning of a frequency disturbance with the proposed adaptive droop coefficient (see Figure 7a,b).

As shown in Figure 7b,d, due to the fact the droop coefficient of the proposed scheme is coupled with the ROCOF, a larger droop control coefficient is obtained according to (10). Therefore, the active power of DFIG implemented with the proposed scheme increases from 52.8 MW to 74.3 MW, and the power increment is 21.5 MW; the active power of the conventional method is increased from 52.8 MW to 71.7 MW, and the incremental power of the conventional is 18.9 MW. As the system frequency returns to quasi steady state, the ROCOF becomes zero, and the active power injected into the electric power system by the proposed scheme is same as that by the conventional scheme after 80 s (see Figure 7b).

Based on the above-mentioned explanations, the conventional (ROCOF) scheme would not be compared with the proposed scheme in the following cases due to the less performance in terms of frequency nadir improvement.

5.3. Case 3: Wind Speed of 8.5 m/s and Disturbance of 120 MW

The wind speed and wind power penetration for this case are same as that in Case 1, and the disturbance is twice that of Case 1.

As displayed in Figure 8, the maximum ROCOF and FN for the MPPT operation are -0.700 Hz/s and 59.033 Hz, respectively, which are worse than that of Case 1 due to the increased disturbance. For the conventional and proposed strategies, the frequency nadirs respectively increase to 59.247 Hz and 59.274 Hz/s, and the maximum ROCOF increases to -0.679 Hz/s and -0.666 Hz/s, respectively due to a certain amount of the kinetic energy is fed to the power grid. Moreover, compared to the conventional scheme, the maximum ROCOF and FN are improved by 0.013 Hz/s and 0.027 Hz, respectively when the DFIGs adopt the proposed scheme. Hence, the maximum ROCOF and frequency nadir improvements of the proposed droop control scheme for Case 2 is greater than that of Case 1 because the droop control coefficient is a function of the ROCOF, which increases with the ROCOF (see Figure 8c).

Furthermore, the peak output power of the proposed strategy is higher compared that of the conventional scheme so that the FN of the proposed strategy is better (see Figure 8b,c).

5.4. Case 4: Random Wind Conditions and Disturbance of 120 MW

For this case, the performances of the proposed scheme are validated with random wind condition whose wind speed curve is shown in Figure 9a, and the wind power level and frequency disturbance are same as Case 2. Figure 9 displays the simulation results for Case 3.

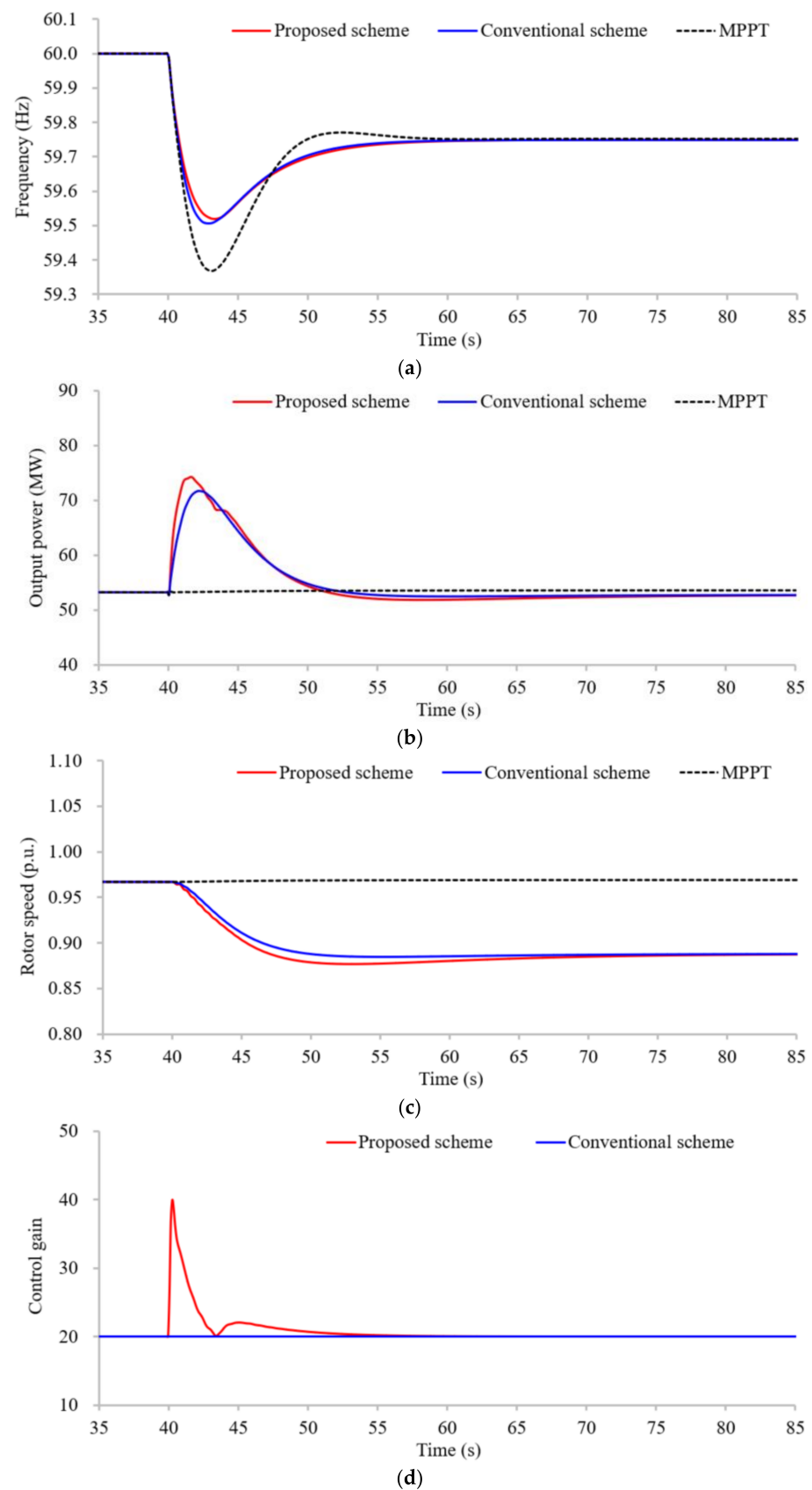


Figure 8. Simulation results for Case 3: (a) System frequencies; (b) Active power of the DFIG; (c) Rotor speeds; (d) Control coefficients.

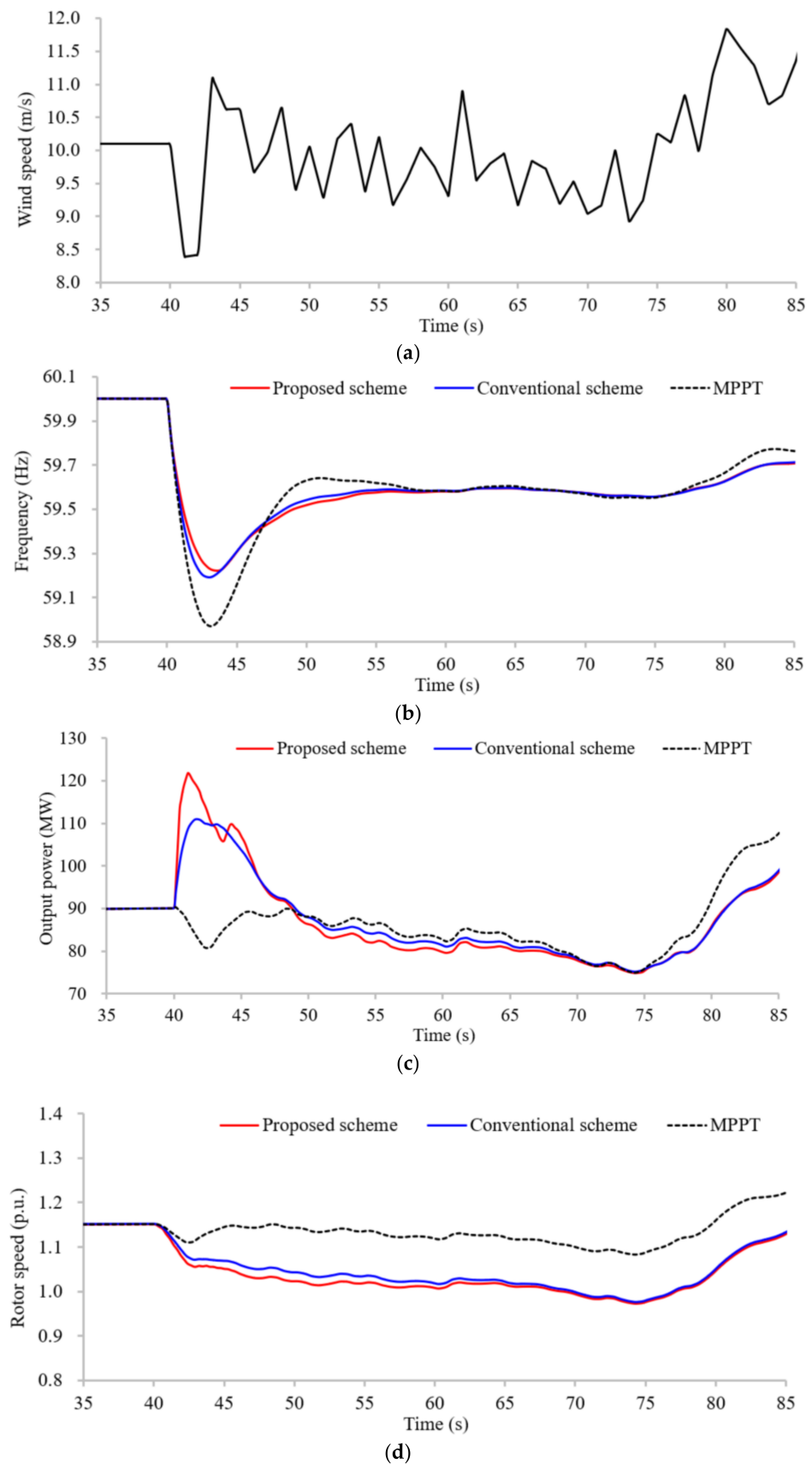


Figure 9. Simulation results for Case 4: (a) Wind speed; (b) System frequencies; (c) Active power of the DFIG; (d) Rotor speeds.

From Figure 9a, it can be seen that the FNs of the proposed scheme, conventional scheme, and MPPT operation are 59.222 Hz, 59.191 Hz, and 58.970 Hz, respectively, and the frequency nadirs of three control schemes is all lower than those of Case 2 due to the wind speed drop. The maximum ROCOFs of the proposed scheme, conventional scheme, and MPPT operation are -0.660 Hz/s, -0.674 Hz/s, and -0.696 Hz/s, respectively. The maximum ROCOF of the proposed scheme is less than those of the MPPT operation and the conventional scheme by 0.036 Hz/s and 0.014 Hz/s, respectively. As in Case 2, the proposed scheme can further boost the frequency nadir and reduce the maximum ROCOF compared to the conventional droop control scheme. This is because more energy of the DFIG is fed to the power grid (see Figure 9c). Furthermore, the frequency nadir improvement of the proposed droop control scheme is greater than that of the conventional droop control scheme, since the droop control coefficient is a function of the ROCOF.

For all cases, the proposed scheme shows much better performance than the conventional scheme and MPPT mode in terms of alleviating the maximum ROCOF and boosting the frequency nadir under various disturbances and wind speed conditions. In addition, for the proposed scheme, the improvements of the maximum ROCOF and frequency nadir under a severe disturbance is better than that under a small one compared the results of Case 2 to Case 3.

6. Conclusions

This article suggests an enhanced droop control strategy to improve the frequency response capability more effectively in response to various frequency disturbances. To this end, an adaptive droop control coefficient based on the rate of change of frequency (ROCOF) is designed. The performances of the proposed droop control strategy were investigated on EMTP-RV with various disturbances and wind conditions. The advantages of this strategy as follows:

- (1) The proposed control droop coefficient is coupled with the ROCOF which can reflect the size of the disturbance. Furthermore, a power function to regulate the control coefficient. Thus, the proposed droop control scheme can adaptively adjust the frequency response capability under various disturbances.
- (2) Based on the fixed control gain for the conventional scheme, a supplementary function of the ROCOF is suggested. Thus, the proposed scheme can generate more power to improve the frequency-supporting capability of the DFIG.

Simulation results on various disturbances and wind speed conditions clearly imply that the proposed droop control strategy shows better performances than the conventional scheme in terms of heightening the FN and reducing the maximum ROCOF, especially in a serve frequency event. Future research will focus on investigating the inertial control scheme of the large-scale wind farm considering the wake effects.

Author Contributions: Conceptualization, D.Y. and X.Z.; methodology, D.Y. and Y.X.; software, Y.X. and P.C.; validation, Y.X., D.Y. and X.Z.; formal analysis, X.Z. and P.C.; investigation, X.Z. and P.C.; resources, Y.X. and D.Y.; data curation, Y.X. and P.C.; writing—original draft preparation, Y.X., P.C., D.Y. and X.Z.; writing—review and editing, Y.X., P.C., D.Y. and X.Z.; visualization, X.Z.; supervision, X.Z.; project administration, D.Y. and X.Z.; funding acquisition, D.Y. and X.Z. All authors have read and agreed to the published version of the manuscript.

Funding: This work was supported in part by the National Natural Science Foundation of China (51877112), the Natural Science Foundation of the Jiangsu Higher Education Institutions of China (20KJB470026 and 20KJA470002), Nantong Science and Technology Research Project (MS22020022 and JC2020094).

Data Availability Statement: Not applicable.

Conflicts of Interest: The authors declare no conflict of interest.

Nomenclature

β	Pitch angle
ω_s	Rotor speed of the grid
i_r	Current at rotor circuit
i_s	Current at stator circuit
I_r	Current at rotor circuit for dq-axis
I_s	Current at stator circuit for dq-axis
u_g	Voltage at GSC
i_g	Current at GSC
U_g	Grid voltage for dq-axis
I_g	Grid current for dq-axis
U_{dc}	Voltage at DC-link
U_{dc}^*	Reference voltage at DC-link
Q_g	Reactive power at GSC
Q_g^*	Power reference at GSC
I_{gd}^*	current reference at GSC for d-axis
I_{gq}^*	current references at GSC for q-axis
Q_s^*	Reactive Power reference at RSC
c_p	Power coefficient
S	Swept area
λ	Tip-speed ratio
B	Pitch angle
v_w	Wind speed
R	Blade length
λ_{opt}	Optimal tip-speed ratio
T_{em}	Mechanical torque from the turbine
T_e	Generator electrical torque
H_t	Turbine inertia constant
H_g	Generator inertia constant
T_{ls}	Torques of the low-speed shaft
T_{hs}	Torques of the high-speed shaft
ω_t	Turbine rotor speed
ω_r	Generator rotor speed
K	Spring constant
θ_s	Torsional twist
D	Damping constant
ω_{ls}	Rotor angular velocity of the low-speed shaft
P_{MPPT}	Output of MPPT operation
ΔP_{droop}	Incremental power for the droop control loop
K_{AG}	Adaptive gain
Δf	Frequency deviation
K_0	Basic control coefficient for the droop control
k_1	Droop control factor
DFIGs	Doubly-fed induction generators
ROCOF	Rate of change of frequency
TSGs	Traditional synchronous generators
FN	Frequency nadir
RSC	Rotor-side controller
GSC	Grid-side controller
MPPT	Maximum power point tracking
RSC	Rotor-side controller
GSC	Grid-side controller
EMPT-RV	Energy Management Training Program, Restructured Version

References

1. Bevrani, H. *Robust Power System Frequency Control*, 2nd ed.; Springer: New York, NY, USA, 2014.
2. Yang, D.; Kim, J.; Kang, Y.C.; Muljadi, E.; Zhang, N.; Hong, J.; Song, S.-H.; Zheng, T. Temporary Frequency Support of a DFIG for High Wind Power Penetration. *IEEE Trans. Power Syst.* **2018**, *33*, 3428–3437. [\[CrossRef\]](#)
3. Jeon, H.; Kang, Y.C.; Park, J.-W.; Lee, Y.I. PI Control Loop-Based Frequency Smoothing of a Doubly-Fed Induction Generator. *IEEE Trans. Sustain. Energy* **2021**, *12*, 1811–1819. [\[CrossRef\]](#)
4. Yang, D.; Jin, Z.; Zheng, T.; Jin, E. An adaptive droop control strategy with smooth rotor speed recovery capability for type III wind turbine generators. *Int. J. Electr. Power Energy Syst.* **2022**, *135*, 107532. [\[CrossRef\]](#)
5. Dai, J.; Tang, Y.; Wang, Q.; Jiang, P. Aggregation Frequency Response Modeling for Wind Power Plants with Primary Frequency Regulation Service. *IEEE Access* **2019**, *7*, 108561–108570. [\[CrossRef\]](#)
6. Nguyen, H.; Yang, G.; Nielsen, A.; Jensen, P. Combination of Synchronous Condenser and Synthetic Inertia for Frequency Stability Enhancement in Low-Inertia Systems. *IEEE Trans. Sustain. Energy* **2019**, *10*, 997–1005. [\[CrossRef\]](#)
7. Ackermann, T. *Wind Power in Power Systems*, 2nd ed.; John Wiley & Sons, Ltd.: Chichester, UK, 2012.
8. Yang, D.; Gao, H.-C.; Zhang, L.; Zheng, T.; Hua, L.; Zhang, X. Short-term frequency support of a doubly-fed induction generator based on an adaptive power reference function. *Int. J. Electr. Power Energy Syst.* **2020**, *119*, 105955. [\[CrossRef\]](#)
9. Miller, N.W.; Shao, M.; Venataraman, S. *California ISO: Frequency Response Study*; GE Energy: Paris, France, 2011. Available online: <http://www.caiso.com/Documents/Report-FrequencyResponseStudy.pdf> (accessed on 10 October 2021).
10. Keung, P.-K.; Li, P.; Banakar, H.; Ooi, B.T. Kinetic Energy of Wind-Turbine Generators for System Frequency Support. *IEEE Trans. Power Syst.* **2008**, *24*, 279–287. [\[CrossRef\]](#)
11. Muljadi, E.; Gevorgian, V.; Singh, M.; Santoso, S. Understanding inertial and frequency response of wind power plants. In Proceedings of the 2012 IEEE Power Electronics and Machines in Wind Applications, Denver, CO, USA, 16–18 July 2012; pp. 1–8.
12. Engleitner, R.; Nied, A.; Cavalca, M.S.M.; Da Costa, J.P. Dynamic Analysis of Small Wind Turbines Frequency Support Capability in a Low-Power Wind-Diesel Microgrid. *IEEE Trans. Ind. Appl.* **2018**, *54*, 102–111. [\[CrossRef\]](#)
13. Ochoa, D.; Martinez, S. Fast-Frequency Response Provided by DFIG-Wind Turbines and its Impact on the Grid. *IEEE Trans. Power Syst.* **2017**, *32*, 4002–4011. [\[CrossRef\]](#)
14. Kheshti, M.; Ding, L.; Bao, W.; Yin, M.; Wu, Q.; Terzija, V. Toward Intelligent Inertial Frequency Participation of Wind Farms for the Grid Frequency Control. *IEEE Trans. Ind. Inform.* **2019**, *16*, 6772–6786. [\[CrossRef\]](#)
15. Hydro Québec TransÉnergie. *Transmission Provider Technical Requirements for the Connection of Power Plants to the Hydro Québec Transmission System*; TransÉnergie: Montréal, QC, Canada, 2009.
16. National Grid UK, Grid Code Review Panel Paper, Future Frequency Response Services. September 2010. Available online: <https://www.nationalgrid.com/sites/default/files/documents/15575-Future%20Frequency%20Response%20Services.pdf> (accessed on 10 October 2021).
17. Gevorgian, V.; Zhang, Y.; Ela, E. Investigating the Impacts of Wind Generation Participation in Interconnection Frequency Response. *IEEE Trans. Sustain. Energy* **2015**, *6*, 1004–1012. [\[CrossRef\]](#)
18. Garmroodi, M.; Verbic, G.; Hill, D.J. Frequency Support from Wind Turbine Generators with a Time-Variable Droop Characteristic. *IEEE Trans. Sustain. Energy* **2017**, *9*, 676–684. [\[CrossRef\]](#)
19. Abouzeid, S.I.; Guo, Y.; Zhang, H.C. Improvements in primary frequency regulation of the grid connected variable speed wind turbine. *IET Renew. Power Gener.* **2019**, *13*, 491–499. [\[CrossRef\]](#)
20. Xi, J.; Geng, H.; Zou, X. Decoupling Scheme for Virtual Synchronous Generator Controlled Wind Farms Participating in Inertial Response. *J. Mod. Power Syst. Clean Energy* **2021**, *9*, 347–355. [\[CrossRef\]](#)
21. Sun, M.; Min, Y.; Chen, L. Optimal auxiliary frequency control of wind turbine generators and coordination with synchronous generators. *CSEE J. Power Energy Syst.* **2021**, *7*, 78–85.
22. Ye, H.; Pei, W.; Qi, Z. Analytical Modeling of Inertial and Droop Responses from a Wind Farm for Short-Term Frequency Regulation in Power Systems. *IEEE Trans. Power Syst.* **2015**, *31*, 3414–3423. [\[CrossRef\]](#)
23. Morren, J.; de Haan, S.W.H.; Kling, W.L.; Ferreira, J.A. Wind Turbines Emulating Inertia and Supporting Primary Frequency Control. *IEEE Trans. Power Syst.* **2006**, *21*, 433–434. [\[CrossRef\]](#)
24. Hu, Y.-L.; Wu, Y.-K. Approximation to Frequency Control Capability of a DFIG-Based Wind Farm Using a Simple Linear Gain Droop Control. *IEEE Trans. Ind. Appl.* **2019**, *55*, 2300–2309. [\[CrossRef\]](#)
25. Li, Y.; Xu, Z.; Wong, K.P. Advanced Control Strategies of PMSG-Based Wind Turbines for System Inertia Support. *IEEE Trans. Power Syst.* **2017**, *32*, 3027–3037. [\[CrossRef\]](#)
26. Van De Vyver, J.; De Kooning, J.D.M.; Meersman, B.; Vandeveld, L.; Vandoorn, T.L. Droop Control as an Alternative Inertial Response Strategy for the Synthetic Inertia on Wind Turbines. *IEEE Trans. Power Syst.* **2015**, *31*, 1129–1138. [\[CrossRef\]](#)
27. Lee, H.; Kim, J.; Hur, D.; Kang, Y.C. Inertial Control of a DFIG-based Wind Power Plant using the Maximum Rate of Change of Frequency and the Frequency Deviation. *J. Electr. Eng. Technol.* **2015**, *10*, 496–503. [\[CrossRef\]](#)
28. Lorenzo, Z.; Andreas, J.R.; Janus, M.-S.; Ioannis, M.; Anca, D.H.; Poul, S. Virtual inertia for variable speed wind turbines. *Wind Energy* **2013**, *16*, 1225–1239.
29. Ramtharan, G.; Ekanayake, J.B.; Jenkins, N. Frequency support from doubly fed induction generator wind turbines. *IET Renew. Power Gener.* **2007**, *1*, 3–9. [\[CrossRef\]](#)

30. Zhao, J.; Lyu, X.; Fu, Y.; Hu, X.; Li, F. Coordinated Microgrid Frequency Regulation Based on DFIG Variable Coefficient Using Virtual Inertia and Primary Frequency Control. *IEEE Trans. Energy Convers.* **2016**, *31*, 833–845. [[CrossRef](#)]
31. Wu, Y.-K.; Yang, W.H.; Hu, Y.L. Frequency regulation at a wind farm using a timing-varying inertia and droop controls. *IEEE Trans. Ind. Appl.* **2019**, *55*, 213–2224. [[CrossRef](#)]
32. Yoo, J.I.; Kang, Y.C.; Muljadi, E.; Kim, K.-H.; Park, J.-W. Frequency Stability Support of a DFIG to Improve the Settling Frequency. *IEEE Access* **2020**, *8*, 22473–22482. [[CrossRef](#)]
33. Ye, R.-J.; Li, H.; Chen, Z.; Gao, Q. Comparison of transient behaviors of wind turbines with DFIG considering the shaft flexible models. In Proceedings of the 2008 International Conference on Electrical Machines and Systems, Wuhan, China, 17–20 October 2008; pp. 2585–2590.
34. Anderson, P.M.; Mirheydar, M. A low-order system frequency response model. *IEEE Trans. Power Syst.* **1990**, *5*, 720–729. [[CrossRef](#)]
35. Akbari, M.; Madani, S.M. Analytical evaluation of control strategies for participation of doubly fed induction generator-based wind farms in power system short-term frequency regulation. *IET Renew. Power Gener.* **2014**, *8*, 324–333. [[CrossRef](#)]
36. Kundur, P. *Power System Stability and Control*; McGraw-Hill Inc.: New York, NY, USA, 1994.
37. Tielens, P.; Hertem, D.V. Grid Inertia and Frequency Control in Power Systems with High Penetration of Renewables. In Proceedings of the Young Researchers Symposium in Electrical Power Engineering, Delft, The Netherlands, 16–17 April 2012.